EUROPEAN FUSION DEVELOPMENT AGREEMENT

EFDA–JET–PR(05)22

A. Zabolotsky, H. Weisen, A. Karpushov, TCV Team
and JET EFDA contributors

Influence of Particle Sources on Electron Density Peaking in TCV and JET

Influence of Particle Sources on Electron Density Peaking in TCV and JET

A. Zabolotsky, H. Weisen, A. Karpushov, TCV Team
and JET EFDA contributors*

Centre de Recherches en Physique des Plasmas, Association EURATOM - Confederation Suisse,
Ecole Polytechnique Federale de Lausanne CH-1015 Lausanne, Switzerland
** See annex of J. Pamela et al, "Overview of JET Results ",*
(Proc. 20th IAEA Fusion Energy Conference, Vilamoura, Portugal (2004).

Preprint of Paper to be submitted for publication in
Nuclear Fusion

ABSTRACT.
Calculations of the particle flux caused by neutrals originating from the edge are performed for TCV and JET, using the one dimensional kinetic transport code Kn1D. The analysis, confirmed by experimental evidence, shows that for TCV and for JET, edge fuelling as well as neutral beam fuelling cannot be responsible for density gradient in the plasma bulk, confirming the presence of inward particle convection. The results corroborate the expectation of a peaked density profile in ITER, despite the lack of bulk particle fuelling.

1. INTRODUCTION

The nature of the peaked electron density profiles in tokamaks has been the subject of controversy for a long time [1]. Recent experiments in fully current driven plasmas with negligible particle source in Tore Supra [2] and TCV [3] have shown that substantial peaking is obtained in the absence of the neoclassicalWare pinch [4] ($V_{Ware} \propto E_{tor}/B_{pol}$), providing an unambiguous demonstration of the existence of anomalous inward pinches. At the same time, a study of JET H-mode discharges suggested [5] that the effect of edge fuelling may not be negligible, as usually assumed and may contribute to density peaking to the same extent as NBI fuelling. In this paper we present a detailed analysis of the processes of neutral penetration and the role of the edge neutrals for electron density peaking in the TCV (R_0 = 0.88m, a < 0.25m, I_p < 1.1MA) and the JET (R_0 = 2.96m, avert 2.1m, I_p < 6MA) tokamaks.

For a deuterium (or hydrogen) plasma in steady state, the electron ne and neutral n0 densities within the closed flux surfaces can be described by fluid transport equations

$$\nabla(-D\nabla n_e + V \cdot n_e) = n_e n_0 S_{ion} - n^2_e S_{rec} \quad (1)$$

Influence of particle sources on electron density peaking in TCV and JET 2

$$\nabla(n_o v_0) = -n_e n_0 S_{ion} + n^2_e S_{rec} \quad (2)$$

where V is the radial flow velocity (pinch velocity), v_0 is the neutral fluid velocity, S_{ion} is a rate coefficient for ionization of neutrals by electron impact, S_{rec} is the rate coefficient for radiative recombination and D is the particle diffusivity within the closed flux surfaces. These equations show that the presence of the particle source term directly influences the density gradient in regions where the source is important. Ionization of neutral particles in the core produces radial density gradients and as seen from the equations above, the term $n_e n_0 S_{ion}$ has a similar influence on the density profile as an inward pinch. Therefore the neutral particle source has to be considered as a possible candidate for peaked density profiles.

The potential sources of neutral particles in tokamak plasmas are neutrals produced by recycling, neutrals produced by recombination and neutrals injected by neutral heating beams. In the absence of neutral beams, the majority of the neutral influx comes from recycled deuterium released from

the wall protection tiles (carbon in TCV and JET), which cover the inside of the tokamak vessel and are thus located at the edge.

These neutrals are initially cold and have a short mean free path. Deep fuelling by edge neutrals is possible via charge exchange processes with hot plasma ions, which produce fast neutrals, which can penetrate from the edge to the bulk plasma. Neutral beam injection used for plasma heating represents an addition to the edge recycling source of neutral particles. The beam neutrals are characterized by high energy (~105 eV for JET) and therefore can penetrate in to the plasma core. The location of the particle source produced by the beam and its strength depend on the beam deposition profile and have to be calculated for each discharge using numerical codes.

2. PENETRATION OF NEUTRALS

There are several reactions which are important in creation of ionized particle sources or sinks in hydrogen plasmas [6]:

$$\begin{aligned} &\text{a) } e^- + H_2 \rightarrow e^- + H^+_2 + e^- \\ &\text{b) } e^- + H \rightarrow e^- + H^+ + e^- \\ &\text{c) } H_2 + e^- \rightarrow H + H + e^- \\ &\text{d) } H + H^+ \rightarrow H^+ + H \\ &\text{e) } H^+ + e^- \rightarrow H + h\nu \end{aligned} \qquad (3)$$

The two major processes which lead to ionization of neutral hydrogen coming from the periphery are direct ionization of the molecular hydrogen (a) and ionization of the atomic hydrogen (b). Important processes which do not lead directly to creation of additional charged particles but determines the concentration of neutrals are dissociation of molecular hydrogen and the creation of Frank-Condon atoms (c) and charge exchange of atomic deuterium (d). A sink for hydrogen ions in the plasma is provided by radiative recombination (e). Reaction rate coefficients as a function of temperature for the reactions listed in (3) are shown on Fig. 1 [7]. It is seen from the comparison of Influence of particle sources on electron density peaking in TCV and JET 3 Figure 1. A) and B) Rate coefficients for atomic processes in hydrogen [7]. The labelling corresponds to the reactions listed in (3) Fig. 1A and B that radiative recombination of hydrogen atoms can play a role only in high density plasmas, since the rate coefficient of this process is significantly lower than the ionization and charge exchange rate coefficients. In the energy range above 100eV , the recombination rate coefficient is smaller by 6 orders of magnitude than the rate coefficient for charge exchange or ionization. Consequently, in regimes with low electron densities the main source of the neutral particles is the flux from the wall.

The neutral concentration in the plasma is therefore determined by a balance between neutrals entering the plasma from the wall and the ionization. This balance depends on the velocity of neutrals, their concentration and on the density of the electrons. For a particle with velocity v, the mean free path can be estimated as

$$\lambda = \frac{\upsilon}{n < \sigma \upsilon >},$$

where £mv is the rate coefficient for the processes considered and n is the plasma electron or ion density. For the electron temperature range $20 < T_e < 400$eV , typical for conditions just inside the Last Closed Flux Surface (LCFS), the rate coefficient for processes leading to the direct ionization of molecular hydrogen are larger than $2 \cdot 10^{-8}$ m^3/s. For densities near the LCFS, which are usually in the range $0.5 - 5 \cdot 10^{19}$ m^{-3} and typical thermal velocities of $2 \cdot 10^3$ m/s, the penetration length of molecular hydrogen λ is 1cm or less. This penetration depth is rather small compared to the minor radius of TCV (25cm) or JET (1m) and therefore the contribution of the molecules to density peaking is small beyond the vicinity of the LCFS.

For Frank-Condon atoms, which result from molecular dissociation, with an average energy of 2eV , the mean free path is still only of the order of 1 cm at the high end of the density range, (at which molecular deuterium is not expected to penetrate beyond the LCFS), but may be as high as 10cm at the lowest edge densities, which include many of the TCV ECH plasmas. Moreover, unlike molecules, neutral atoms can penetrate in a diffusive-like manner by a sequence of charge exchange processes, until an ionization occurs. Charge exchange of slow neutral particles with fast plasma ions creates slow ions

Influence of particle sources on electron density peaking in TCV and JET 4 Figure 2. Kn1D geometry (Kn1D manual [8]) and fast neutral particles. Energetic neutrals can have penetration lengths comparable to the size of the plasma and therefore can be ionized or undergo subsequent charge exchange reactions further inside the LCFS. The CX process is indeed important because the resonant charge exchange cross section is higher than the ionization cross section.

Several CX reactions can occur before ionization, leading to an effective acceleration of the neutral particles.

The importance of CX neutrals depends on the ratio of neutral atomic fluxes to the molecular fluxes as well as on the plasma background conditions and normally requires specific codes to estimate. To perform this estimation we had two tools in our disposal: the one dimensional kinetic transport code Kn1D [8] and two dimensional transport code DOUBLE-TCV.

Kn1D computes the neutral atomic and molecular hydrogen (or deuterium) distribution functions (f_H,f_{H_2}) in a slab-like spatial geometry with specified plasma profiles. The model geometry in Kn1D consists (in increasing values of x) of a wall surface, a local limiter shadow, a plasma Scrape-Off Layer (SOL) region and a core plasma (Fig.2). The numerical algorithm includes charge exchange collisions, electron-impact ionization and dissociation, elastic self-collisions (atomic and molecular), and a variety of elastic cross-collisions (atom-ion, atom-molecule, molecule-ion).

The DOUBLE-TCV code uses a Monte-Carlo technique to calculate neutral distributions in the plasma, assuming a plasma column surrounded by a homogenous atomic gas density, specified by atomic neutral density and energy for each species defined at the last closed surface. The plasma

geometry is introduced into the code as a poloidal flux map (R,Z). The code generates the following outputs: 2D distributions of neutral density of each mass species in the poloidal plane; neutral densities and emissivity distributions.

We compared the results of calculation of neutral densities inside LCFS performed by DOUBLE-TCV and Kn1D codes in several TCV discharges. For example, profiles of neutral density in Ohmic TCV discharge are shown in Fig.3. Two codes give very similar results for $\rho_{pol} > 0.6$ and diverge, although not by more than a factor of two, at the plasma centre. Based on this comparison, we concluded that for the purpose of numerical treatment of neutral flux the bulk plasma simplified kinetic 1D code can be used. Another advantage of Kn1D code for present study is the ionization source as an output, the quantity which can be compared with outward plasma flux and the importance of particle source in particle balance equation can therefore be estimated.

3. PARTICLE SOURCES IN TCV

TCV does not have a neutral beam heating system and therefore there are only two sources of neutrals in limited discharge: the flux of neutral atoms from the walls and the radiative recombination of the plasma bulk ions. The diagnostic neutral ion beam used to measure $T_i(\rho)$ has an insignificant total source rate ~10^{19} s^{-1} and was not yet available for most of the experiments described in this work.

3.1. KN1D SIMULATIONS FOR TCV

In defining the Kn1D geometry for TCV discharges the following assumptions were made. A limiter configuration with an inner wall as a limiter surface was chosen (see Fig.4). In this case the neutral hydrogen recycling form a wall tends to be ionized inside the LCFS. Accordingly the SOL length was chosen to be equal to zero. The outer wall was assumed to serve as a wall in the Kn1D geometry and the length of limiter shadow was taken equal to 2cm.

The background plasma electron density $n_e(\rho)$ and electron temperature $T_e(\rho)$ profiles inside the LCFS, where ρ is square root of normalized poloidal flux, were taken from Thomson scattering measurements [9]. Outside the LCFS, the temperature and density profiles were assumed to have an exponential decay leading to wall temperatures of the order of 10–20eV and densities 2–3 times below the values at LCFS in accordance with Langmuir probe data [10]. Ion temperature profiles in the plasma bulk were approximated using data from charge exchange spectroscopy [11]. Outside the LCFS, an exponential decay of ion temperatures similar to that of the electron temperature decay was assumed. All profiles were remapped to the 1D coordinate along the axis x on Fig. 4 using the discharge equilibrium data.

The result of a Kn1D simulation as a function of distance along the x axis (Fig.4) for a TCV Ohmic L-mode discharge is shown on Fig.5. This discharge has a very low central electron density $n_e(0)$ ~$8 \cdot 10^{18}$ m^{-3} and represent practically the lowest density of the TCV operational domain. The densities of molecular deuterium and of neutral atoms, the temperature of neutral atoms and the

atomic ionization rate are shown on Fig.5 by dashed lines. The atomic ionization rate plotted on Fig.5d corresponds to the term $n_e n_0 S_{ion}$ in Eq. (1). Profiles of electron and ion temperatures are shown in Fig.5 by solid lines. It is seen that the heating of the electrons by the Ohmic current and strong decrease of energy exchange between ions and electrons at low density results in a large difference, more than a factor of four, between ion and electron temperatures. As it was predicted by a simple estimation at the beginning of this chapter, the density of molecular atoms drops down very rapidly with the distance from the limiter and the corresponding flux can be neglected over most of the cross section. The main part of the neutral flux inside LCFS is due to atomic neutrals and as seen from the changes of the simulated temperature of atoms, neutral particles penetrate in a diffusivelike manner increasing their energy in successive charge exchange processes. This increase of the energy of the neutrals leads to slower changes of the atomic ionization rate nen0Sion Åfi(n0v0) with respect to the decrease of n_0.

To understand the importance of particle flux term in the particle balance equation, the simulated particle flux due to the edge source

$$\Gamma_{source} = \int \left(n_e n_0 S_{ion} - n_e^2 S_{rec} \right) dl \qquad (4)$$

was compared with an outward diffusive flux $\Gamma_D = -D\nabla n_e$, where ∇n_e is the experimental density gradient and D is the diffusion coefficient. D was chosen to be a parabolic function $D = \rho^2 + 0.1$ m^2/s with a non zero value at the centre. In steady state conditions and in absence of convection the total flux $\Gamma = \Gamma_D + \Gamma_{source}$ should be equal to zero.

To make a comparison we performed several simulations with different values of pressure at the wall, P_{wall}, which is a free parameter in Kn1D. In an ideal situation, this value should correspond to the vessel pressure. However in a real experiment, the complexity of walls and limiter geometry and uncertainties in molecular-atomic processes in the SOL do not allow us to determine this absolute density of the neutral molecules at the wall with sufficient accuracy. Some constraints can come from a comparison of the measured H_{alpha} emission with the Kn1D simulation, but the poloidal asymmetry of the observed H_{alpha} emission make this comparison quite ambiguous. Another difficulty is that H_α diagnostics lack the resolution that would be required to distinguish between emission inside and outside the LCFS, only the former being indicative of plasma fuelling.

In Fig.6 a comparison of Γ_D obtained using experimental density profiles and Γ_{source} calculated by Kn1D is shown. The curve a) correspond to an exact match of Γ_{source} and £FD at the edge, which implies the absence of a radial pinch at $\rho = 1$ in steady state. Similarly two other curves correspond to situations when inward (curve b) or outward (curve c) pinches are present at LCFS.

Due to the large difference in the slope of Γ_D and Γ_{source}, it is not possible to satisfy the particle balance equation without invoking convective processes. It is clearly seen that for the case of curve a) in Fig.6, Γ_D and Γ_{source} match only at the edge. At $\rho \sim 0.6$ source flux due to ionization of neutral particles is smaller by a factor of 2.5 than the diffusive flux. In the plasma centre this difference is

close to a factor 10. Therefore neutral particle penetration from the edge cannot be responsible for density profile steepness and an additional inward pinch term is needed to compensate the diffusive flux in steady state conditions.

It has to be noted that the absolute values of D chosen for the diffusive flux has no influence on the results of the comparison because of the above mentioned renormalization of Γ_{source}. However the profile of D is important. Measurements of D are difficult and were not available for this work. Taking into account the fact that measured by perturbative techniques, profiles of the diffusion coefficient in L-mode tokamak discharges usually rises more slowly than ρ^2 [12, 13, 14, 15], the choice of a parabolic function gives the lower limit to the plasma particle flux profile and therefore increase the influence of edge particle source. If the profile of D is flatter than ρ^2, the difference between Γ_D and Γ_{source} is even more important than in the example presented in Fig.6. We should note, however, that with a steeper than ρ^2 profile of D, the Γ_D and Γ_{source} may be comparable over the entire discharge.

If an inward pinch is present at the LCFS (curve b) in Fig. 6, the difference between Γ_{source} and Γ_D becomes more significant than for the case of curve a) not only at the edge, but in the bulk as well. The example of curve c) shows that if an outward pinch is present at LCFS it must change direction at some point inside the plasma in order to keep the total flux zero at each radial position. The point of pinch reversal would depend on the values of the pinch at the edge, the diffusion coefficient, the plasma density and temperature profiles. We are not aware of any physical mechanism which can produce such a behaviour of the pinch velocity.

The previous example shows that at low densities the concentration of the neutral particles n_0 and as a consequence particle source $S_p \sim n_0 n_e < \sigma_v >_{ion}$ in the plasma bulk is determined by CX process. The mean free path of the neutrals after charge exchange depends on the energy of the plasma ions, which in turn is determined by the plasma ion temperature. Additionally, a higher energy of neutral particles increases the associated flux (see Eq. (2)). Therefore it is important also to analyze discharges with high ion temperature.

During the Ohmic heating the ions are heated via electron-ion collisions and the local power transmitted from electrons to ions can be estimated as

$$P_{ei} = \frac{3}{2} n_i \frac{dT_i}{dt} \propto n_e^2 \, ¥ \, \frac{T_e - T_e}{T_e^{3/2}},$$

The transfer of energy to ions is more efficient for plasmas with high electron density and this fact is confirmed by ion temperature measurements in TCV.

To perform a simulation with Kn1D we chose a discharge close to the maximum density available on TCV: $n_e(0) \sim 1.7 \cdot 10^{20}$ m^{-3}. The electron temperature was measured to be 650eV at maximum and ion temperature was estimated from CSXR measurements [11] to be as high as 580eV at the centre.

The results of the simulation are presented in Fig.7 where all definitions are the same as for

Fig.5. The density of molecular deuterium drops by two orders of magnitude already in the limiter shadow and the associated flux can be completely neglected inside the LCFS. As in the case of the low density discharge, neutral atoms penetrate in a diffusive like manner increasing their temperature practically to 580 eV in the plasma centre. However the increase of the CX rate due to the high temperature cannot compensate for the strong decrease of the mean free path due to the density increase. The density of neutral atoms drops exponentially by four order of magnitude in first ten centimeters inside the LCFS and remains nearly constant from that point up to the centre. This constancy of the neutral concentration is explained by recombination. The neutral particle concentration resulting from recombination is determined by the following expression

$$n_0 \simeq \frac{<\sigma\upsilon>_{rec}}{<\sigma\upsilon>_{ion}} \cdot n_i \qquad (5)$$

For electron temperatures of order of 500eV the ratio $<\sigma v>_{rec} / <\sigma v>_{ion} \simeq 2 \cdot 10^{-8}$ and for ion densities $n_i \simeq 1 \cdot 10^{20}\,m^{-8}$, the concentration of neutral atoms due to recombination, $n_0 \simeq 5 \cdot 10^{12}\,m^{-8}$, is comparable with concentration of wall neutrals transported to the plasma bulk by CX process (see. Fig. 7c). From this point the concentration of the neutral particles in plasma no longer depends on the neutral flux from the wall, since the latter becomes several orders of magnitude weaker than the flux from recombination of plasma ions.

The results of a comparison of the outward diffusive flux with the particle flux created by neutral atoms is presented on Fig.8. The particle flux created by neutrals still remains significantly low. In the central regions of the plasma, where recombination is important, the particle source flux becomes zero Eq. (5) and Eq. (1). These results indicate that the particle source from the edge cannot account for density peaking in TCV high density discharges.

Other important domains of TCV operation are Ohmic H-mode discharges and discharges with ECH heating. Ohmic H-mode discharges on TCV have central densities higher than $6 \cdot 10^{19}\,m^{-3}$ and the conclusions of the simulation presented on Fig.7 and 8 are valid. ECRH discharges are characterized by high electron temperatures (several keV) and low central electron densities (typically $1 \div 3 \cdot 10^{19}\,m^{-3}$). In these conditions the electron-ion coupling is strongly reduced and ion temperatures remain low ($T_i(0) \sim 200 - 400$keV) [11]. Therefore, the neutral penetration is similar to the neutral penetration in the low density discharge presented in Fig.5 and Fig.6.

3.2. EXPERIMENTAL EVIDENCE OF NEUTRAL PENETRATION ON TCV

As predicted by the simple formula for the mean free path of edge neutrals and observed in the more complex diffusive like behaviour, the penetration of the neutrals is dependent on the absolute value of electron density. Kn1D simulations performed for plasma parameters taken from Pulse No: 25174, show that for fixed profiles of electron temperature and for fixed plasma shape, ratio of $-\Gamma_D/\Gamma_{source}$ at $\rho_{pol} = 0.7$ is an exponential function of the central density in the range $n_e(0) = 0.8 \cdot 10^{18} - 6 \cdot 10^{19}\,m^{-3}$

$$\frac{-\Gamma_D(0.7)}{\Gamma_{source}(0.7)} \sim e^{0.8 \cdot n_e(0)/10^{19}}$$

For central densities higher than $6 \cdot 10^{19}$ m^{-3} recombination starts to play a role and the dependence on the $n_e(0)$ disappears. However, for such densities the ratio $-\Gamma_D/\Gamma_{source}$ at $\rho_{pol}(0.7)$ is already close to 100 and therefore Γ_{source} can be neglected. As a result, one experimental test for the importance of edge neutrals in the formation of electron density gradients is a comparison of profiles with different central densities.

Two examples of normalized profiles of electron density in Ohmic L-mode discharges with similar plasma current and shape are shown in Fig.9(a) and (b). All discharges have practically the same peaking of electron density at fixed current, completely independent of the absolute values of the density. Even the lowest density discharge, which represents a typical target for ECRH scenarios, shows no additional peaking in comparison with highest density discharge (Fig.9). Therefore we can conclude that the experimental data show no evidence for the importance of edge neutral penetration, thereby confirming the conclusion drawn from Kn1D simulations.

Another way of experimentally assessing the effect of the edge source is a comparison of the electron density peaking in deuterium and helium plasmas. The ionization crosssection is higher in He than in H and the charge-exchange cross-section is much lower.

This combination of these properties should lead to a significant reduction of the fast CX neutral flux and hence of deep fuelling.

Helium can exist as an neutral atom, as an ion with charge +1 or it can be completely ionized. Charge exchange is possible on both stages: He^+ and He^{++}. The rate coefficients of the processes in He are shown on Fig.10. The double CX rate coefficient is more than four times lower in He than in H (see Fig.1 for comparison). At the same time cross-section of ionization of the atoms is only 1.5 times smaller in He than in H. Therefore the ratio $<\sigma v>_{CX}/<\sigma v>_{ion}$ for He is equal to 1/5 at 100eV that is 10 times lower than the same ratio in H. It means that CX chains are practically absent in He plasmas, and no significant deep fuelling is to be expected.

We did not have at our disposal a transport code for atoms and ions able to treat a pure He plasma and in order to understand the difference in neutral penetration between H and He discharges we performed the following reasoning. Neutral atoms with an initial density n_0 (left of the diagram 11), directed towards the plasma core from the edge can be ionized, experience charge exchange with fast plasma ions and create fast neutral atoms or penetrate as cold neutrals into the plasma. The branching ratios for the different processes are determined by the corresponding rate coefficients. Assuming a fixed electron density, ion and electron temperatures along the penetration path, we can estimate the decay of the initial concentration and the final concentration of fast neutral particles which contribute to core fuelling. The reactions corresponding to the left part of the diagram are the following: $He^{++} + He \rightarrow He + He^{++}$ (double charge exchange) with the rate $\nu_{doubleCX} = n_e \cdot <\sigma v>_{doubleCX}/2$ and $e + He \rightarrow e + He^+ + e$ (ionization of He) with the rate $\nu_{ion} = n_e \cdot <\sigma v>_{ion}$. For both

rates $n_{He++} = n_e/2$ was assumed. For ion and electron temperatures of about 200eV typical for Ohmic L-mode TCV discharges in the region $\rho_{pol} \sim 0.8 - 0.9$ the total ionization rate exceeds the rate of double charge exchange by factor of 5 and therefore the probability of ionization is four times higher than creation of fast neutral via CX. Assuming an exponential decay of the densities with the distance and taking into account the relations

$$-dn_0(x) = dn_H(x) + dn_{0fast}(x),$$

$$\frac{dn_{0fast}(x)}{dn_{H++}(x)} = \frac{\lambda_{ion}}{\lambda_{CX}},$$

we can estimate the densities of n_{He+} ions and fast neutrals n_{01fast} at a distance $x_1 = \lambda_{CX}$:

$$n_{0fast} = \frac{n_0 \lambda_{CX}}{\lambda_{ion}\left(1 + \frac{\lambda_{CX}}{\lambda_{ion}}\right)}\left\{1 - exp\left(-\frac{x}{\lambda_{CX}} - \frac{x}{\lambda_{ion}}\right)\right\} \sim 0.15 \cdot n_0 \quad (6)$$

$$n_{He^+} = \frac{n_0}{\lambda_{ion}\left(1 + \frac{\lambda_{CX}}{\lambda_{ion}}\right)}\left\{1 - exp\left(-\frac{x}{\lambda_{CX}} - \frac{x}{\lambda_{ion}}\right)\right\} \sim 0.6 \cdot n_0 \quad (7)$$

Since the density of He^{++} at $\rho_{pol} \simeq 0.8 - 0.9$ is significantly higher than the density of He+ produced by the edge neutrals, the single CX process and the resulting density of fast neutrals (top right of the Fig.11) can be completely neglected. At this stage, thefast neutral can be produced only by double CX on the cold neutrals having penetrated from the edge or fast neutrals created from the preceding double CX. The probability distribution between ionization products (ions) and double CX products (neutrals) can be again estimated using (6) and (7).

Summarizing above we can see that at temperatures about $200eV$ and at the distance $2\lambda_{CX}$ less than 20% of initial neutral concentration n_0 will give rise to fast neutrals and more than 80% will be ionized. For comparison, in deuterium plasma at the same distance more than 80% of initial cold atoms will create fast ions in charge exchange reactions. Thus, the different atomic physics in *He* and *H* plasmas results in significant difference in formation of fast CX neutrals and should lead to the difference in profiles of electron density in identical discharges performed in *He* and *H* if neutrals originating from the edge contribute to the density peaking.

He plasmas with ratios of *He/*(*He +D*) higher than 90 % at high electron density were obtained in TCV [16]. Ohmically heated, diverted configurations were performed with a steady state flat top of 1*s*. The electron density profiles, remapped on ρ_{pol} for two He discharges with different current and central densities, together with their deuterium counterparts are shown on Fig.12. Assuming that the source term in (1) is important and taking into account the analysis presented above one should expect flatter density profiles in *He* discharges than in *D* discharges. Evidently, both examples, representing

high density and low density discharges, show no sign of flattening of profiles when *He* is the working gas, thus proving again the insignificance of edge neutrals for the formation peaked density profiles.

4. PARTICLE SOURCES IN JET

The large size of JET ($a \sim 0.85m$) would require a multi-step CX chain, which would results in neutral energies, after CX with hot plasma ions, as high as the ion temperature. Auxiliary heating on JET leads to ion temperatures comparable to or high than the electron temperatures, attaining several *keV* at the plasma centre and high ion temperatures can be obtained even at low densities by neutral beam injection. Compared with TCV, the increase of the flux due to the energy increase might compensate the decrease of neutral densities due to the large machine size.

The next sections present the results of Kn1D simulations performed for JET, as well as experimental results indicating the unimportance of edge source in density peaking. The presence of an additional source of neutral particles due to the neutral heating beams is also discussed.

4.1. KN1D SIMULATIONS FOR JET L-MODE PLASMAS

JET has a complex scrape-off layer with multiple non toroidally symmetric limiters used during the OH phase. Moreover, most JET discharges have a diverted configuration. These conditions make one dimensional simulations of the edge plasma very inaccurate. However, since the main interest of the study is the particle source term inside LCFS the following simplifications in the construction of the 1D geometry were made. The lengths of the SOL and the limiter shadow were chosen to be equal to $5cm$ and the distance along the shortest chord from the limiter to the plasma centre was chosen as a grid for Kn1D. In fact, the details of the geometry outside the LCFS influence the shape of calculated particle source only a few cm inside the LCFS and for large machines such as JET, the inaccuracy in the definition of the geometry does not affect the results in plasma bulk.

The electron temperature profiles are taken from LIDAR TS measurements and the ion temperature was taken from CXS measurements [17]. The density profile was obtained using the SVD-I method [18]. The density outside the LCFS was assumed to decrease exponentially with a distance according to [19]. All profiles were remapped to a one dimensional coordinate along the chord passing from edge to the plasma centre in the midplane using the equilibrium code EFIT [20].

Figure 13 shows experimental density and temperature profiles and simulation results for an L-mode JET discharge in limiter phase heated only with the LH system (this discharge is characteristic of experiments presented in the study of electron density peaking in JET [21]). According to the LIDAR measurements the central density is $n_e(0) \sim 1.3 \cdot 10^{19}\ m^{-3}$ and the central electron temperature is 3keV. The ion temperature inferred from the CXS measurements is lower than the electron temperature. Vertical lines on the Fig.13 mark the LCFS and limiter position in the chosen 1D geometry for Kn1D.

The simulation shows that the large size of JET with respect to TCV results in complete ionization of molecular hydrogen already in the SOL region. The rate of decrease of the neutral density with

distance is similar to the rate obtained for TCV. This results in smaller concentration of the neutral hydrogen at JET than on TCV at the same ρ. Diffusive like penetration via charge exchange of neutral atoms on energetic plasma ions increases the neutral temperature to 1keV in the plasma centre.
A comparison of Γ_D and Γ_{source} similar to the one performed for TCV is shown in Fig.14. The difference between the outward plasma particle flux and the flux created by neutrals coming from the edge is more than one order of magnitude, even in the vicinity of plasma edge and increases toward the centre despite the strong decrease of the diffusive flux. This confirms the unimportance of ìsource in particle balance equation for this type of the discharges.

The results of simulations for high electron and ion temperature JET discharge have to be taken with caution because of limitation of Kn1D atomic cross section data to 800eV beyond which reaction rates are taken as constants. Nevertheless, this restriction does not alter the results since changes in the cross sections for ionization and charge exchange could not account for orders of magnitude difference between Γ_D and Γ_{source} in L-mode discharge. This limitation, however, will strongly influence the results of the simulations in H-mode discharges because of the pedestal region characteristic for H-mode. In the narrow edge pedestal, electron and ion temperatures rise from hundreds of eV to a few keV , well above the 800eV Kn1D limit and hence simulations are not reliable already in the edge region. In order to understand the importance of the source term in H-mode plasmas we relied on the experimental evidence presented in the next section.

4.2. EXPERIMENTAL EVIDENCE OF NEUTRAL PENETRATION ON JET

As in the case of TCV, a pure He plasma in JET is expected to modify the properties of neutral penetration and would give an indication of the importance of multistep CX fuelling processes. We compare electron density profiles from similar JET discharges which were measured in deuterium and helium plasmas. Helium discharges with a purity of nearly 90% were created in the plasma current range 1–2.5MA with neutral heating beam powers up to 12MW [22]. He discharges were chosen to match as closely as possible previous, well characterized D discharges. This allowed to select about 50 pairs of density profiles with very similar discharge conditions and as only difference the working gas. ELMing H - and L - mode phases are equally presented in the selection. Examples of electron density profiles in He and D in L-mode high current discharge and in low current H-mode discharges are presented in Fig.15 and Fig.16 respectively. Details of the profiles in He and D, obtained with the SVD-I method, are in very good agreement with a slight indication of additional peaking in He. Density profile peaking factor defined as $n_e(0)/<n_e>$ s, where <> is the volume average and $n_e(0)$ is central density, in He discharges as a function of peaking factor in D discharges is presented in Fig.17. The diagonal line corresponds to an exact matching of the profile peaking. The central density in the selection is distinguished by classes of symbols and varies by a factor of two from $n_e(0) \sim < 2\cdot10^{19}$ m^{-3} to $n_e(0) \sim 4\cdot10^{19}$ m^{-3}. It is clearly seen that density peaking in some of He discharges is slightly higher than in D discharges as it was noticed in individual profile comparisons. The comparisons of individual profiles and

the independence of peaking on the working gas show the penetration of CX edge neutrals cannot account for density peaking.

4.3. EFFECT OF NEUTRAL BEAM FUELLING IN JET H-MODES

The vast majority of H-mode plasmas in JET are dominated by NBI heating and therefore have a core source of particles, which may be expected to contribute to sustaining density gradients. As for edge neutrals, penetration depends sensitively on plasma density. Interestingly however, density profiles appear not to depend on wether the fuelling profile is peaked or shallow, as seen in Fig.18(a). In this figure two electron density profiles measured by LIDAR TS in the H-mode phase of two discharges are shown. The high density Pulse No: 52823 has a plasma current I_p = 2.5MA, edge safety factor q_{95} =4 and main magnetic field B_t = 2.7T. Only NBI heating with a power of 15.8MW was used. The low density Pulse No: 59301 was heated using 6MW of ICRH power in addition to 8.9MW of NBI power. The plasma parameters are the following: I_p =1.5MA, q_{95} = 4, Bt = 1.7 T. In both discharges the profiles of electron temperature measured by LIDAR TS [23] are practically identical as shown in Fig.18(b). Profiles of ion temperatures (not shown) measured by CXRS are very similar to the electron temperature profiles. Because of the differences in Z_{eff} the two discharges had the same effective collisionality. The difference in the absolute values of the density leads to a strong difference in the particle source from the edge or from heating beams. The profile of the particle source from heating beams was calculated by the PION beam stopping code [24] and plotted by a solid line on Fig.18d. The high density discharge has significantly lower values of atomic ionization rate in the core than the low density discharge and the profile is also different. At the same time the normalized profiles of the electron density (Fig.18(c)) for both discharges are practically identical. The similarity of the electron density profiles is also confirmed by SVD-I method. The identical peaking for the same T_e and T_i, while the density differs by a factor of nearly 3 unambiguously establishes the unimportance of the particle source both from the edge neutrals and from heating beams.

The contribution of beam fuelling to the density gradient in steady state may be estimated as $\nabla n_e/n_e|_{NBI} = \Gamma_{NBI}/Dn_e$. For a typical JET plasma with $n_e \sim 5 \cdot 10^{19}$ m^{-3} and 10MW of NBI heating, the fuelling rate is some 10^{21} s^{-1}, of which some 40% are deposited inside r/a = 0.5, corresponding to $\Gamma_{NBI} \sim 5 \cdot 10^{18}$ m^{-2} s^{-1}. Hence, in order to sustain a typical gradient $\nabla n_e/n_e$ $\nabla < 1$ m^{-1}, D would have to be of order 0.1 m2/s, a low value when compared to heat diffusivity. Unlike heat diffusivity, particle diffusivities cannot be obtained on a routine basis. We therefore relate the beam fuelling contribution to the effective heat diffusivity $\chi = Q/(n_e\nabla T_e + n_i\nabla T_i) \approx Q/(2n_e\nabla T_e)$, where Q is the total heat flux, as follows:

$$\frac{\nabla n_e}{n_e}\Big|_{NBI} = \frac{\Gamma_{NBI}}{Dn_e} - \frac{X}{D} ¥ \frac{T_e}{Q/\Gamma_{NBI}} ¥ \frac{2\nabla T_e}{T_e} \qquad (8)$$

For entirely beam heated plasmas $E_b = Q/\Gamma_{NBI}$ is average the beam energy (100keV at JET). For

typical $|\nabla T_e| / T_e \sim 2\ m^{-1}$ and $T_e \sim 3$keV at mid radius, D would have to be 10 times smaller than χ in order to explain a density gradient $|\nabla n_e| / n_e \sim 1\ m^{-1}$. This is indeed the case for the majority of beam dominated JET H-modes, as seen on Fig.19(a), which plots $|\nabla n_e| / n_e$ versus $\Gamma_{NBI}/\chi n_e$, both of which are evaluated at r/a = 0.5. Γ_{NBI} and Q were obtained using the PION code [24]. The figure contains the data presented in ref [25], augmented by H-modes dominated by Radio-Frequency (RF) heating. The symbols refer to classes of $f_{nb} = Q_{NBI}/Q_{TOT}$. This parameter varies from 0 in purely RF heated plasmas to 1 in purely NBI heated plasmas. The variation of $\Gamma_{NBI}/(\chi n_e)$ for NBI dominated plasmas (red dots) stems not from changes in Γ_{NBI} (because $Q_{NBI}/\Gamma_{NBI} = E_b \approx$ const), but from the range of ∇T_e in the dataset and should therefore not be misinterpreted as a proof that NBI fuelling is the cause of density peaking. As can be seen in the figure, the is no correlation with fnb and hence with Γ_{NBI}/Q_{TOT} . Purely RF heated plasmas maintain finite density gradients which cannot be explained by fuelling, no matter how low a value of D/χ is assumed. These RF plasmas raise the question of whether the Ware pinch [4] may be responsible for density peaking. For TCV L-modes with ECH and EC current drive, the answer to this question has already been found to be no [26, 27]. The Ware pinch V_W is much smaller than ìNBI/ne in beam dominated H-modes and for purely RF heated plasmas a ratio D/$\chi \sim 10^{-2}$ would have to be assumed to explain density gradients in the confinement region. This contrasts with experimental evidence on JET [28] suggesting that D/« is of order unity, at least as far as ions are concerned.

The data presented in Fig.19(a) are clearly not compatible with D/χ of order 10^{-2}. They are however consistent with higher values of D/χ, which implies that beam fuelling can still be a minor contributor to density peaking in JET H-modes. Fig. 19B shows the density peaking factor $n_{e0}/\langle n_e \rangle$ for the same data as Fig.19(a) versus the effective collisionality, which was previously found to be the dominant scaling parameter in JETH modes [25]. We see that RF H-modes are indeed on average some 20% less peaked than their NBI fuelled counterparts, a difference which is of the magnitude expected for NBI fuelling, assuming D/χ in the range 0.5–1. We should note that NBI fuelling may not be the only cause for the difference. A possible alternative candidate or contributor may the reduction of anomalous inward convection due the destabilisation of trapped electron modes by electron heating [29, 30, 27].

SUMMARY

Simulations performed using the one dimensional kinetic transport code KN1D showed that the region over which the source term is important is restricted on TCV and JET, for the discharges considered, to the outermost few cm of the discharge and can be ignored in the particle balance equation in the confinement region. This argumentation is corroborated by the absence of a dependence of the experimental density peaking on the average plasma density and the working gas (D or He) on both machines, which is inconsistent with the large variations with average density or working gas of the penetration depth of the neutrals. The contribution of NBI fuelling to the total density peaking in JET H-mode plasmas was shown to be less than 20%. These results indicate that the main cause for peaked steady state electron density profile in tokamak is

the inward particle pinch and therefore corroborates the conclusion of [25] that peaked density profiles may be expected in ITER, despite the lack of core fuelling.

ACKNOWLEDGEMENTS

The authors would like to thank B. LaBombard for providing the Kn1D code and M.I.Mironov for the DOUBLE-TCV code. This work was partly supported by the Swiss National Science Foundation.

REFERENCES

[1]. F. Wagner and U. Stroth *Plasma Phys. Control. Fusion* **35**, p. 1321, 1993
[2]. G. T. Hoang *et al Phys. Rev. Lett.* **90**, p. 15502, 2003
[3]. I. Furno *et al Phys. Plasmas* **10**, p. 2422, 2003
[4]. A. A. Ware *Phys. Rev. Lett.* **25**, p. 916, 1970
[5]. M. Valoviÿc *et al Plasma Phys. Control. Fusion* **46**, p. 1877, 2004
[6]. P.C. Stangeby and G. M. McCracken *Nucl. Fusion* **30**, p. 1225, 1990
[7]. R. K. Janev *Springer-Verlag, Berlin; New York* 1987
[8]. B. LaBombard ”Manual of Kn1D code””*http://www.psfc.mit.edu/ labombard/*, 2002.
[9]. R. Behn *et al Proc. of the 7th Int. Symp. Laser Aided Plasma Diagnostics, Fukuoka* **30**, p. 392, 2002
[10]. R. Pitts *et al Journal of Nuclear Materials* **290**, p. 940, 2001
[11]. P. Bosshard, *PhD thesis No 2723, Ecole Polytechnique Fédérale de Lausanne, Switzerland*, 2003
[12]. D. R. Baker *et al Nucl. Fusion* **40**, p. 1003, 2000
[13]. K. W. Gentle *et al Nucl. Fusion* **32**, p. 217, 1992
[14]. D. R. Baker *et al Nucl. Fusion* **38**, p. 485, 1998
[15]. J. O’Rourke *Plasma Phys. Control. Fusion* **35**, p. 585, 1993
[16]. I. Condrea *et al Proc. 29th EPS Conference on Controlled Fusion and Plasma Physics, Montreux, Switzerland* **26B**, p. P-2.079, 2002
[17]. M.G. von Hellermann *et al Rev. Sci. Instrum* **61**, p. 3479, 1990
[18]. I. Furno *et al Plasma Phys. Control. Fusion* **47**, p. 49, 2005
[19]. S. K. Erents *et al Nucl. Fusion* **40**, p. 295, 2000
[20]. L. L. Lao *et al Nucl. Fusion* **30**, p. 1035, 1990
[21]. H. Weisen *et al Plasma Phys. Control. Fusion* **46**, p. 751, 2004
[22]. R. Pitts *et al Journal of Nuclear Materials* **313-316**, p. 777, 2003 *Influence of particle sources on electron density peaking in TCV and JET* 23
[23]. C. W. Gowers *et al Rev. Sci. Instrum* **66**, p. 471, 1995
[24]. L-G. Errikson *et al Nucl. Fusion* **33**, p. 1037, 1993
[25]. H. Weisen *et al Nucl. Fusion* **45**, p.L1-L4, 2005
[26]. A.Zabolotsky *et al Plasma Phys. Control. Fusion* **45**, p. 735, 2003

[27]. A.Zabolotsky *et al submitted to Plasma Phys. Control. Fusion*, 2005
[28]. K-D. Zastrow *et al Plasma Phys. Control. Fusion* **46**, p. B255, 2004
[29]. X. Garbet *et al Plasma Phys. Control. Fusion* **46**, p. B557-B574, 2004
[30]. C. Angioni *et al Nucl. Fusion* **44**, p.827, 2004

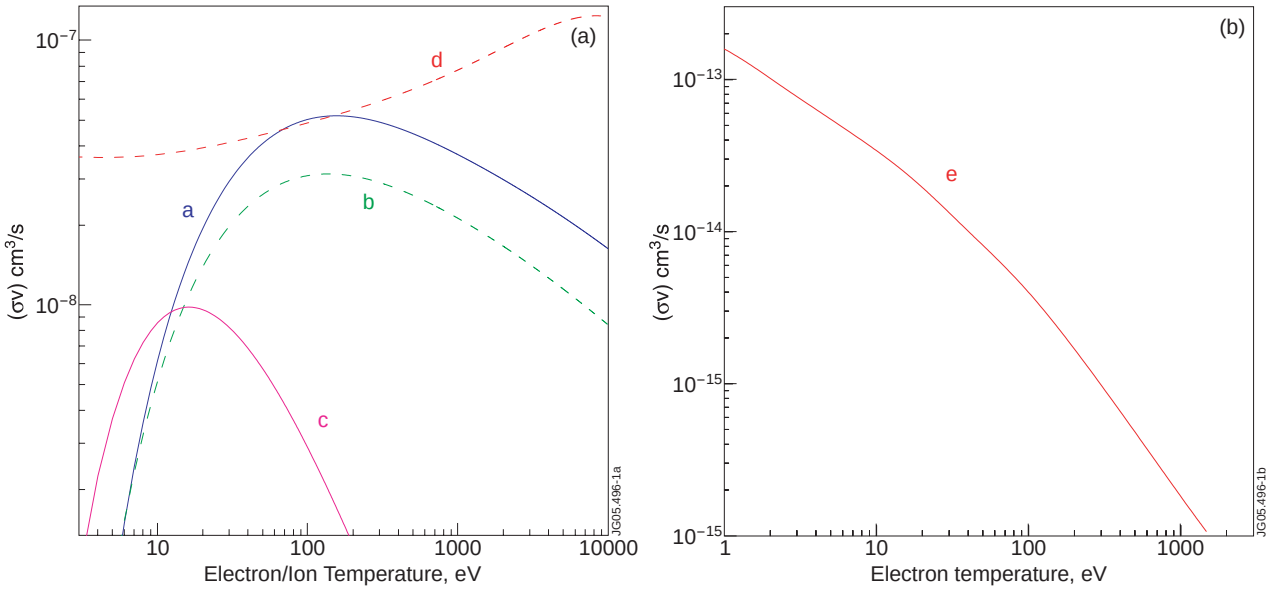

Figure 1: (a) and (b) Rate coefficients for atomic processes in hydrogen [7]. The labelling corresponds to the reactions listed in (3).

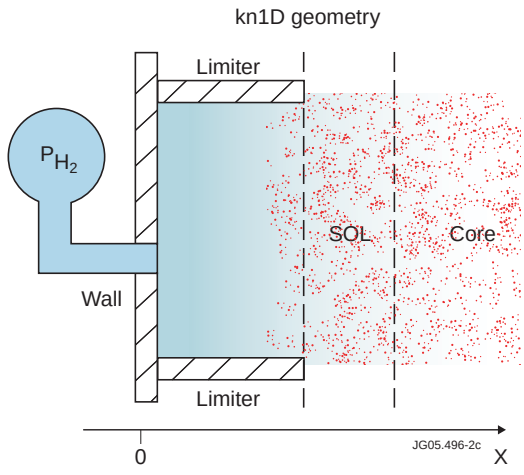

Figure 2: Kn1D geometry (Kn1D manual[8])

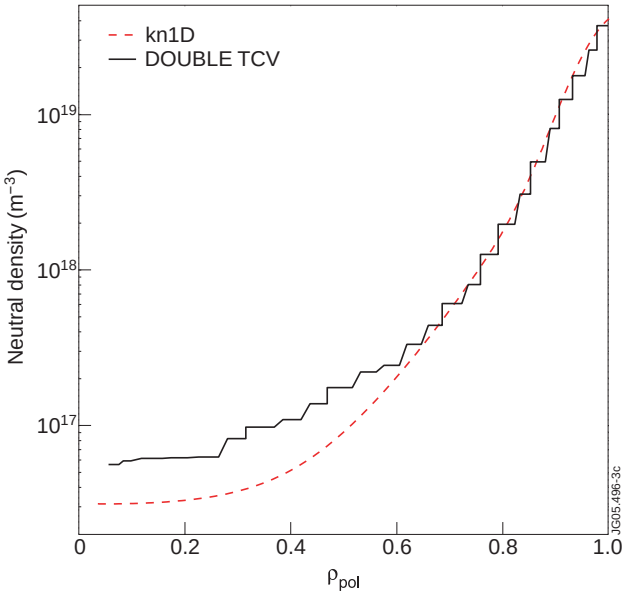

Figure 3. Comparison of neutral densities along ρ_{pol} calculated by Kn1D and DOUBLE-TCV codes.)

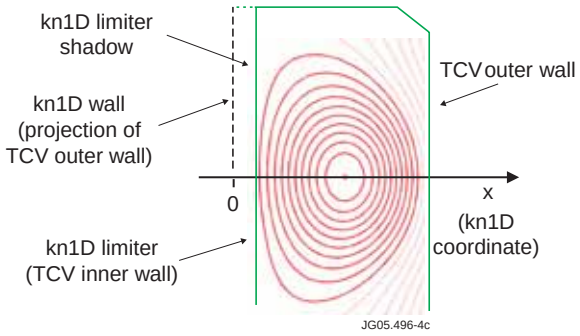

Figure 4: Magnetic flux surfaces, contour of vessel (continuous line) and the elements of Kn1D geometry for a limited TCV discharge.

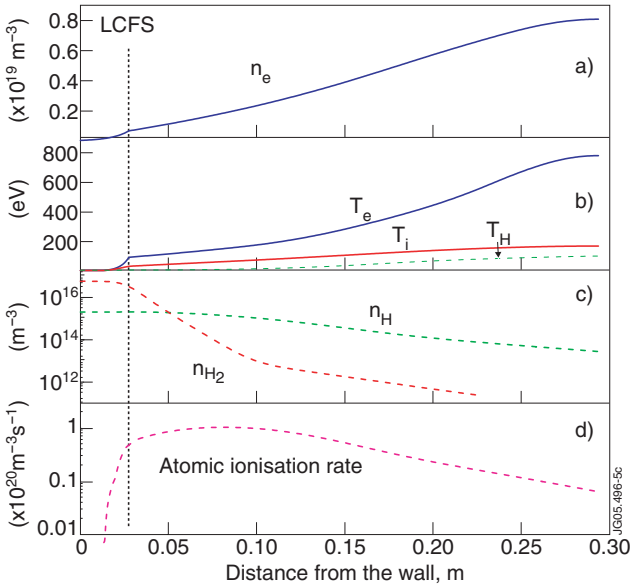

Figure 5: Experimental profiles of electron density a) and electron and ion temperatures b) for the low density Ohmic Pulse No: 25667 as functions of distance from the wall. The results of a Kn1D simulation for temperature of atomic deuterium b), densities of molecular and atomic deuterium c) and atomic ionization rate d) are plotted by dashed lines. The dash-dotted vertical line indicates the position of the LCFS in 1D geometry.

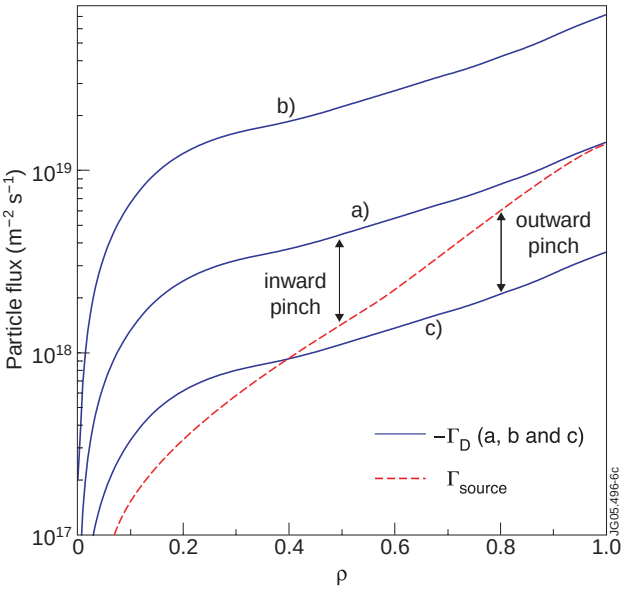

Figure 6: Kn1D Simulation of particle flux Γ_{source} and electron diffusive flux from experimental electron density gradient assuming $D = \rho^2 + 0.1$ for the low density discharge in Fig.5. Lines a) b) and c) represent Γ_D for different values of V ($\rho = 1$) assumed. In steady state, the difference between Γ_{source} and $-\Gamma_D$ require the presence of inward or outward pinch as shown by arrows.

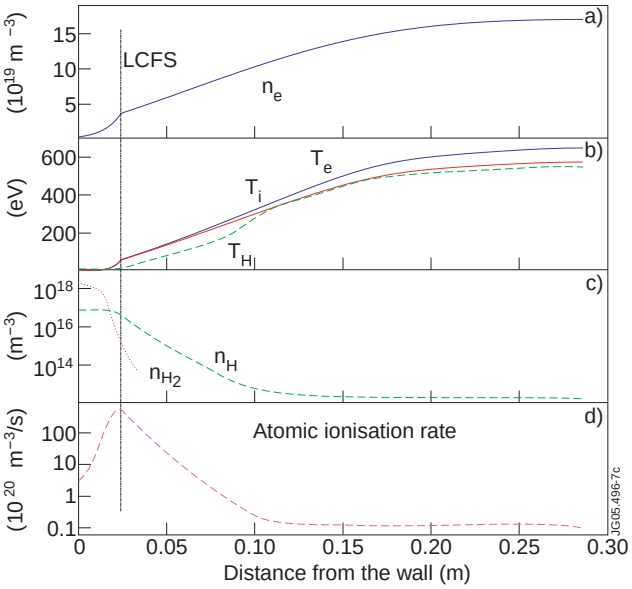

Figure 7: Experimental profiles of electron density a), electron and ion temperatures b) for the high density Ohmic Pulse No: 25174 as functions of the distance from the wall. The results of Kn1D simulation for temperature of atomic deuterium b), densities of molecular and atomic deuterium c) and atomic ionization rate d) are plotted by dashed lines. The dash-dotted vertical line indicates the position of LCFS in projected 1D geometry.

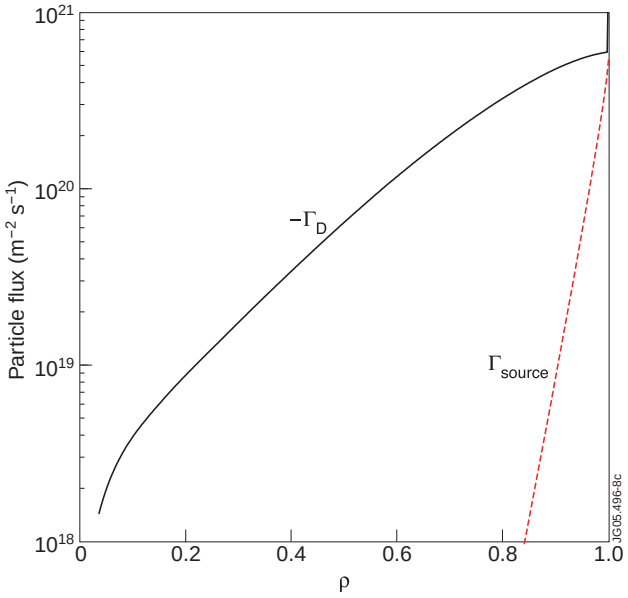

Figure 8: Kn1D Simulation of particle flux Γ_{source} and electron diffusive flux from experimental electron density gradient assuming

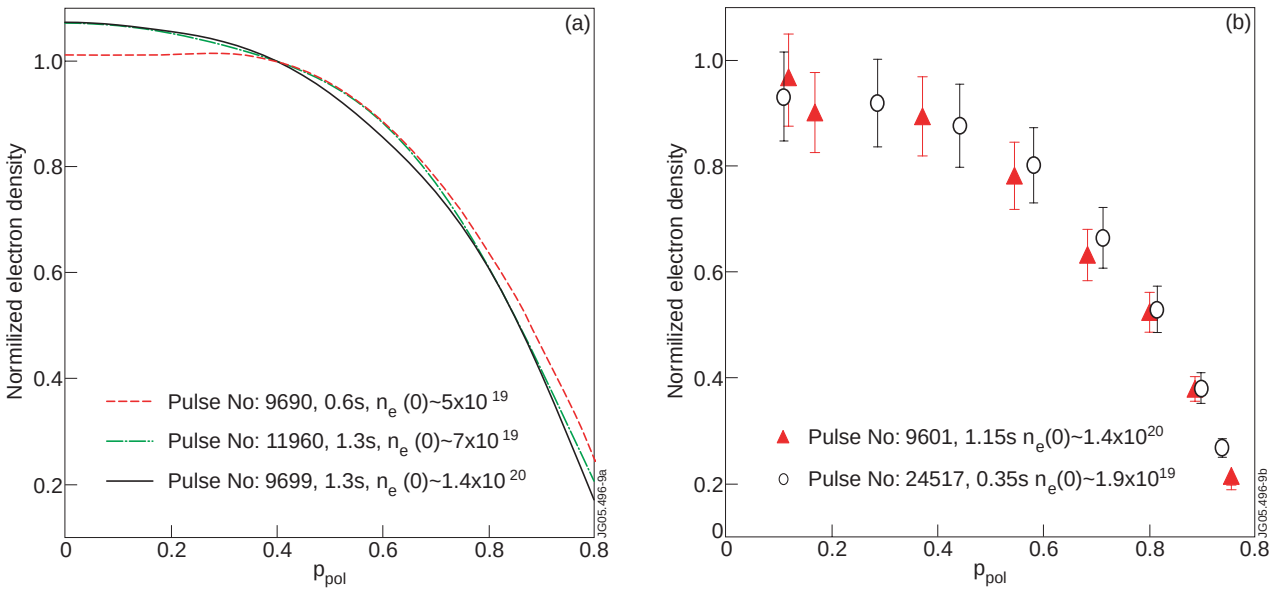

Figure 9: (a) Fitted TS electron density profiles in three Ohmic L mode discharges normalized to the values at inversion radius (plasma current 0.3 MA).(b) TS measurements mapped to ¡pol grid and normalized on central value for two discharges with plasma current 0.22 MA.

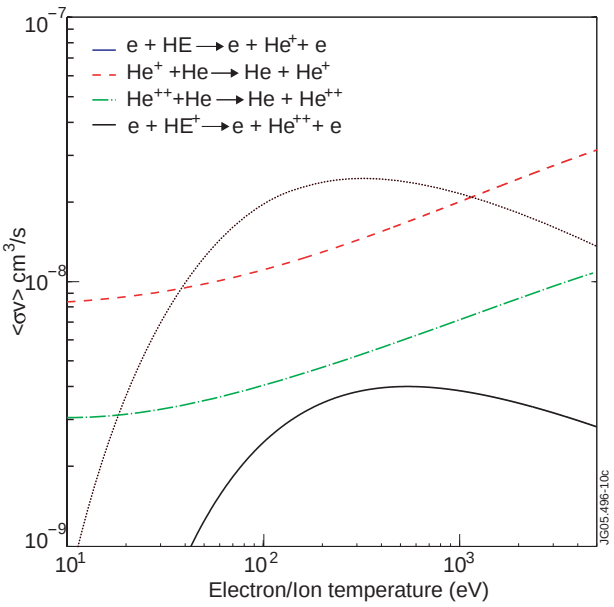

Figure 10: Reaction rate coefficients for important atomic processes in He plasmas

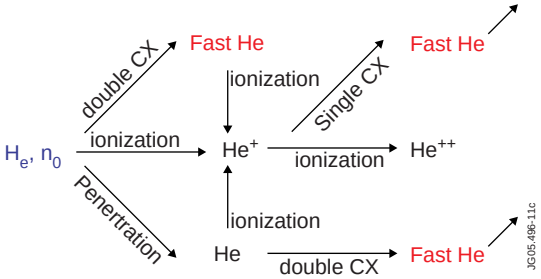

Figure 11. Schematic representation of He penetration

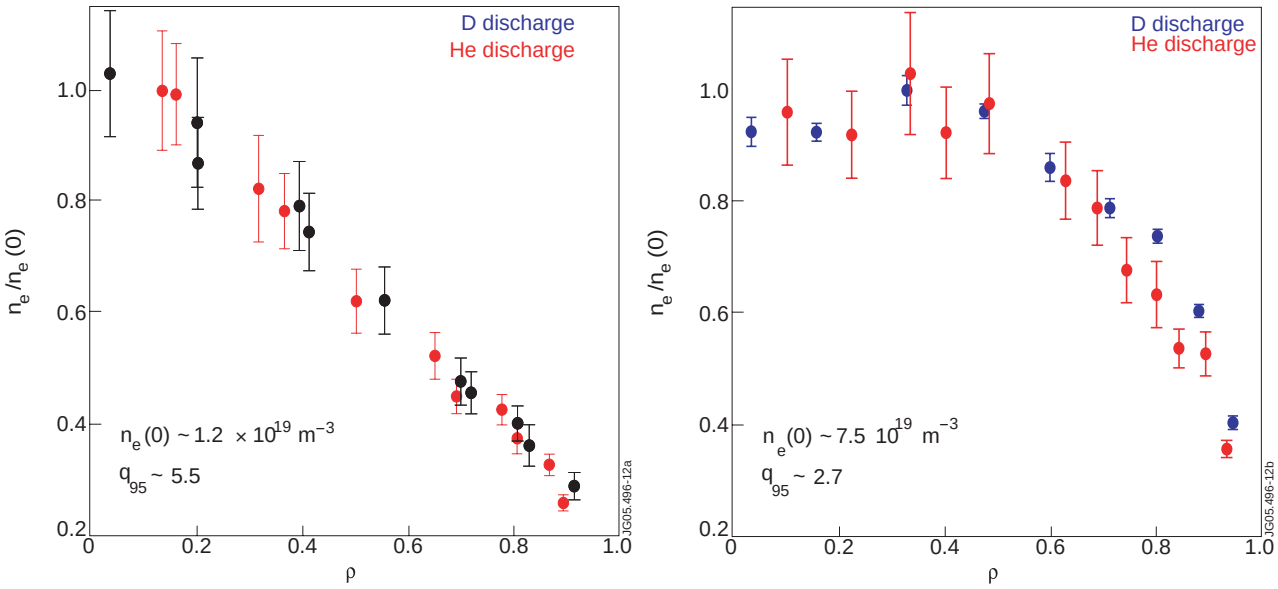

Figure 12: Comparison of the density profiles (left - low density discharge, right -high density discharge) measured by TS in TCV Ohmic He and D plasmas.

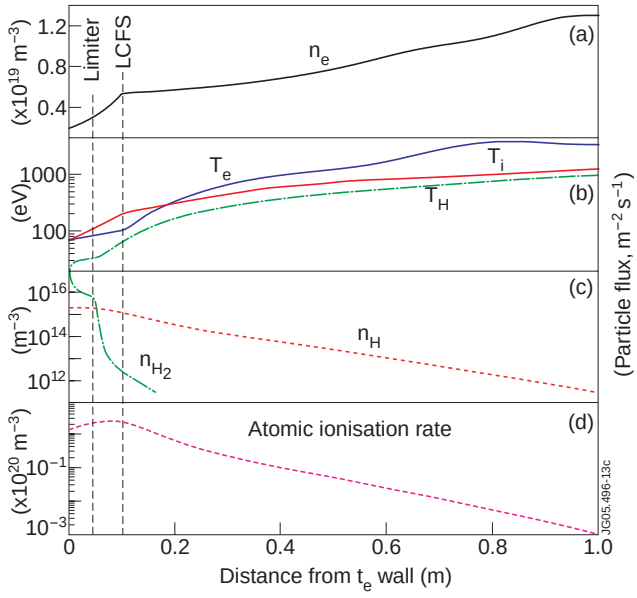

Figure 13: Experimental profiles of electron density a) and electron and ion temperatures b) for the JET L-mode Pulse No: 25667 as functions of distance from the wall. The results of a Kn1D simulation for temperature of atomic deuterium b), densities of molecular and atomic deuterium c) and atomic ionization rate d) are plotted by dashed lines. The dash-dotted vertical line indicates the position of the limiter and LCFS in 1D geometry.

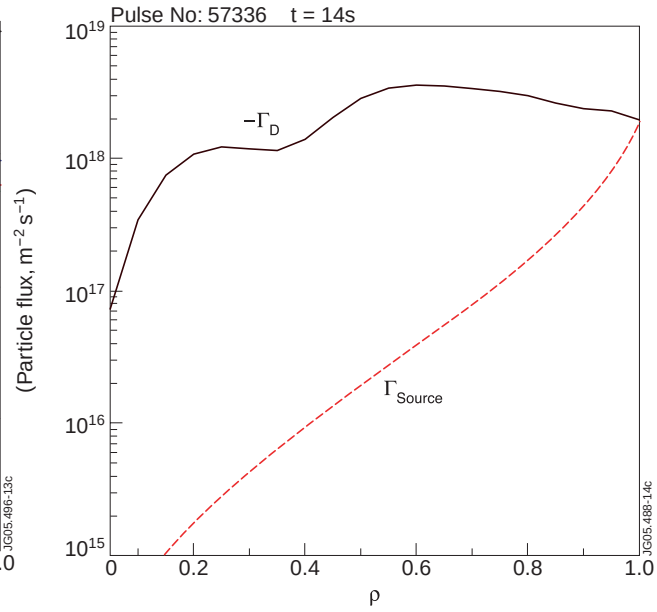

Figure 14. Kn1D Simulation of JET particle flux ìsource and electron diffusive flux ìsource and electron diffusive flux from experimental electron density gradient assuming $D = \rho^2 + 0.1$

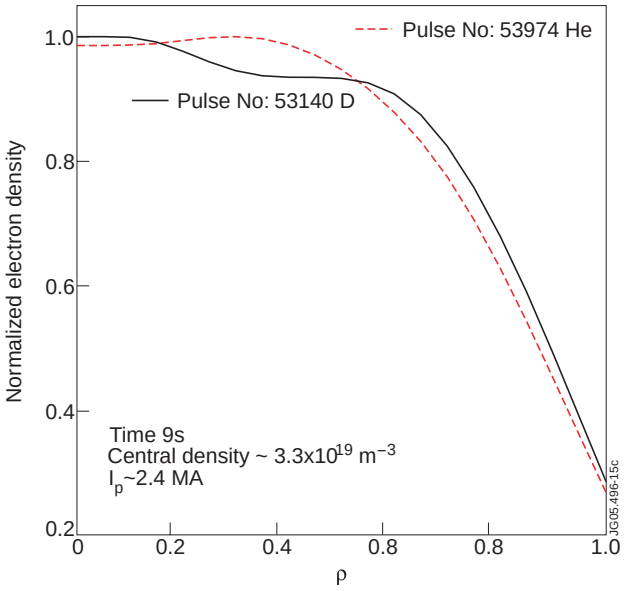

Figure 15. Comparison of electron density profiles in He and D of L-mode high current discharge

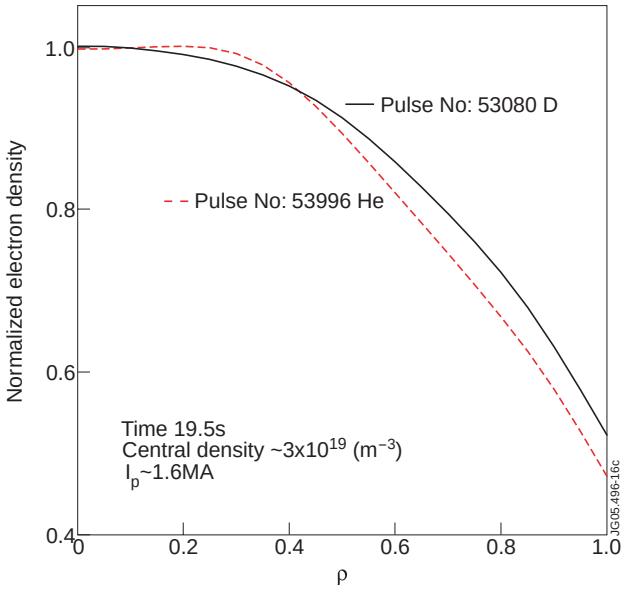

Figure 16. Comparison of electron density profiles in He and D of H-mode low current discharge

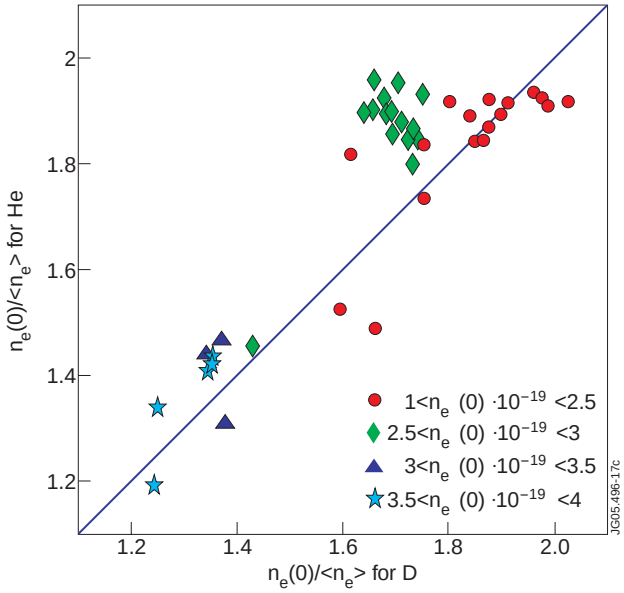

Figure 17: Electron density profile peaking in He discharges compared with peaking in identical D discharge. The line indicates identical profile peaking. The symbols refer to the classes of central density.

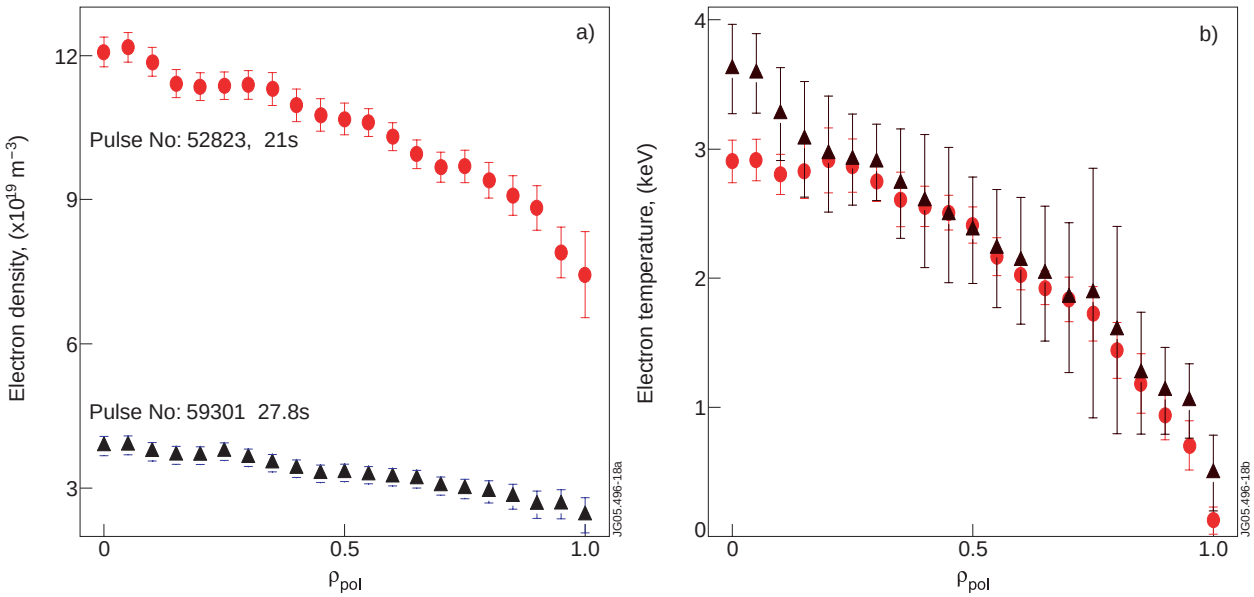

Figure 18. Comparison of two H-mode discharges with different values of centraldensities. (a)and (b) Electron density and electron temperature profiles from Lidar TS measurements.

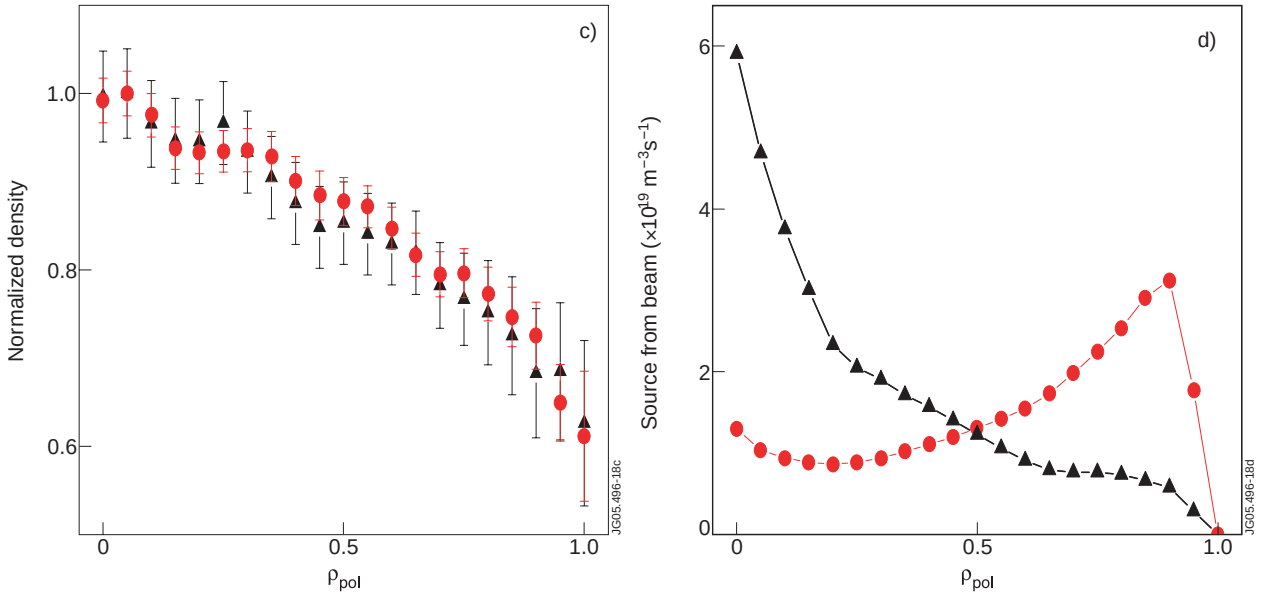

(c). Electron density profiles normalized on central density values. (d) Profiles of particle sources from neutral heating beams.

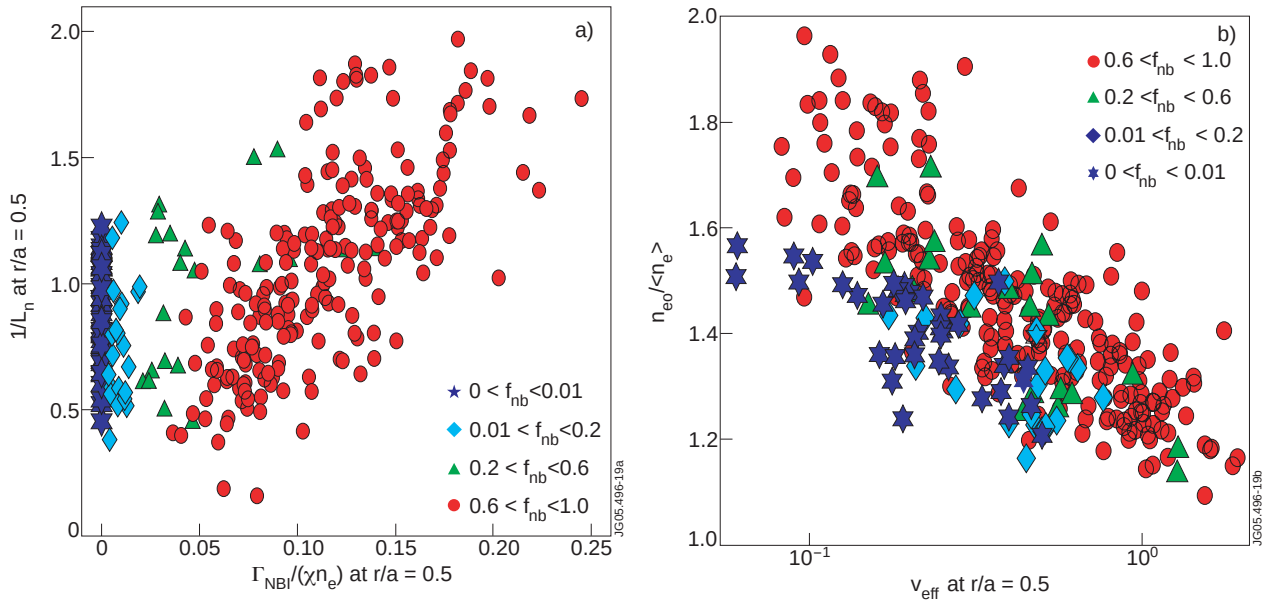

Figure 19: (a) Inverse density gradient length as a function of $\Gamma_{NBI}/\chi n_e$. Symbols indicate the classes of $f_{nb} = Q_{NBI}/Q_{TOT}$. (b) Density peaking factor as a function of effective collisionality (for details see [25]). For both figures the discharges with substantial fraction of NBI heating ($f_{nb} > 0.6$) are identical to those presented in [25].